Heliyon 10 (2024) e27637

Contents lists available at ScienceDirect

Heliyon

journal homepage: www.cell.com/heliyon

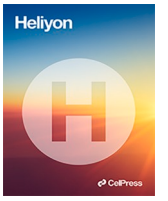

Research article

Morphological changes in perisynaptic astrocytes induced by dopamine neuronal degeneration in the striatum of rats

Liping Sun [a,1], Xuefeng Zheng [b,c,1], Yichen Che [c,1], Ye Zhang [e], Ziyun Huang [b], Linju Jia [b], Yaofeng Zhu [d], Wanlong Lei [b,***], Guoqing Guo [c,**], Chunkui Shao [a,*]

[a] *Department of Pathology, The Third Affiliated Hospital, Sun Yat-sen University, Guangzhou, China*
[b] *Department of Anatomy, Zhongshan School of Medicine, Sun Yat-sen University, Guangzhou, China*
[c] *Department of Anatomy, Neuroscience Laboratory for Cognitive and Developmental Disorders, Medical College of Jinan University, Guangzhou, China*
[d] *Institute of Medicine, College of Medicine, Jishou University, Jishou, China*
[e] *School of Nursing, Sun Yat-Sen University, Guangzhou, China*

ARTICLE INFO

Keywords:
Parkinson's disease
Dopamine neuronal degeneration
Astrocytes
Glutamatergic synapse

ABSTRACT

Introduction: The typical functionality of astrocytes was previously shown to be disrupted by Parkinson's disease (PD), which actively regulates synaptic neurotransmission. However, the morphological changes in astrocytes wrapping glutamatergic synapses in the striatum after dopamine (DA) neuronal degeneration is unclear.

Methods: We utilized a range of methodologies, encompassing the 6-hydroxydopamine (6OHDA)-induced PD model, as well as techniques such as immunohistochemistry, Western blotting, immunofluorescence and immunoelectron microscopy (IEM) to delve into the consequences of DA neuronal degeneration on the morphological attributes of perisynaptic astrocytes.

Results: Our findings demonstrated a notable rise in glial fibrillary acidic protein (GFAP) + astrocyte density and an upregulation in GFAP protein expression within the striatum due to DA neuronal degeneration, coincided with the enlargement, elongation, and thickening of astrocyte protuberances. However, the expression levels of glutamate transporter 1 (GLT1) and glutamine synthetase (GS), which are related to glutamate–glutamine cycle, were significantly reduced. Double immunofluorescence and IEM results indicated that different proportions of vesicular glutamate transporter 1 (VGlut1)+ and vesicular glutamate transporter 2 (VGlut2) + terminals were wrapped by astrocytes. Additionally, DA neuronal degeneration increased the percentage and area of VGlut1+ and VGlut2+ terminals wrapped by GFAP + astrocytes in the striatum. Furthermore, we noted that DA neuronal degeneration increased the percentage of VGlut1+ and VGlut2+ axo-spinous synapses wrapped by astrocytes but had no effect on axo-dendritic synapses.

* Corresponding author. Department of Pathology, The Third Affiliated Hospital, Sun Yat-sen University. No.600, Tianhe Road, Guangzhou, Guangdong, China.
** Corresponding author. Neuroscience Laboratory for Cognitive and Developmental Disorders, Department of Anatomy, School of Medicine, Jinan University. No. 601, Huangpu Avenue West, Guangzhou, Guangdong, China.
*** Corresponding author. Department of Anatomy, School of Medicine, Sun Yat-sen University. No. 74, Zhongshan 2nd Road, Guangzhou, Guangdong, China.
E-mail addresses: leiwl@mail.sysu.edu.cn (W. Lei), tgqguo@jnu.edu.cn (G. Guo), shaochk@mail.sysu.edu.cn (C. Shao).
[1] These authors contributed equally to the research.

https://doi.org/10.1016/j.heliyon.2024.e27637
Received 29 August 2023; Received in revised form 3 March 2024; Accepted 4 March 2024
Available online 5 March 2024

Conclusion: Hence, perisynaptic astrocytes wrapping striatal glutamatergic synapses exhibit substantial morphological and functional alterations following DA neuronal degeneration making them a potential target for therapeutic interventions in PD.

1. Introduction

Parkinson's disease (PD) stands out as among the prevailing neurodegenerative conditions. The cardinal pathology of PD resides in the deterioration of the nigrostriatal dopaminergic pathway, catalyzing a cascade of events that culminate in striatal dopamine (DA) insufficiency. This paucity of DA precipitates the manifestation of clinical manifestations typified by striatal dysfunction, including bradykinesia, rigidity, resting tremor, and equilibrium disruptions [1]. Medium spiny neurons (MSNs) represent the primary neuronal population within the striatum, accounting for 90–95% of all neurons in the striatum. These MSNs are split into direct and indirect pathway neurons, each projecting to unique targets [2,3]. Within the intricate neural matrix, the striatum acts as a crossroads where disparate threads of information intertwine. It hungers for inputs not only from the enigmatic substantia nigra but also from the cortex and thalamus. According to previous research, vesicular glutamate transporter 1 (VGlut1) and vesicular glutamate transporter 2 (VGlut2) serve as key markers, the former mainly originating from the cortex and the latter from the thalamus. VGlut1 paints the portrait of cortical connections, its expression a badge of honor for neurons weaving their intricate patterns within the striatum. Meanwhile, the thalamic afferents, started from the parafascicular nucleus (PFn) and journeying through enigmatic pathways, is narrated by the resonating presence of VGlut2 [4]. In the wake of striatal DA neuronal degeneration, a delicate equilibrium falters, and the once harmonious tango between dopaminergic and glutamatergic afferents transforms into a discordant cadence. Echoing our prior endeavors, the intricacies of the postsynaptic tapestry within striatal glutamatergic synapses come to light, each part a unique canvas bearing the brushstrokes of vulnerability under the influence of DA's absence. Among these revelations, a stark disparity emerges — a tale of spines lost in the dance. The dancers of the indirect pathway, in their vulnerability, relinquish their spines with a more grievous abandonment compared to their direct-pathway counterparts [5]. Preceding inquiries have divulged a significant phenomenon: the depletion of striatal dopamine (DA) yields noticeable increments in the densities and dimensions of VGlut1+ and VGlut2+ terminals. Additionally, the dearth of striatal DA prompts reductions in the total and axospinous terminal fractions of VGlut1+ terminals, while the axodendritic terminal fraction aligns closely with control conditions. In our previous research, we have at length discussed the changes in VGlut1 and VGlut2 terminal density and dimensions in PD model mice [6]. In a nutshell, striatal DA reduction leads to morphological changes in VGlut1 and VGlut2 synapses [7]. However, the mechanism underlying the morphological changes in glutamate synapses induced by striatal dopamine neuronal depletion remains unclear.

In the intricate tableau of classical chemical synapses, the presynaptic membrane, synaptic cleft, and postsynaptic membrane stand as the principal constituents. Recent scholarly endeavors have unveiled a noteworthy revelation—the embrace of numerous synapses within the central nervous system by enigmatic astrocytic entities. These astrocytes, shrouded in their cellular role, emerge as conductors of pivotal significance, orchestrating the symphony of synaptic vitality and the conveyance of neural information [8–11]. An astrocyte exhibits an intricate network of numerous membranous extensions that wrap synapses, enabling bidirectional communication with synaptic neuronal elements. They actively respond to neuronal signals and regulate synaptic transmission, thereby establishing what is known as the 'tripartite synapse' [12]. In the hippocampus, glutamatergic synapses are surrounded by a large number of astrocytes [13]. Astrocyte projections around synapses express excitatory amino acid transporters (EAATs), which absorb more than 80% of glutamate in the synaptic clefts at a very high rate, thereby preventing glutamate accumulation that could cause excitatory damage to neurons [14–16]. In the intricate web of PD pathogenesis, a consequential player emerges—glutamate excitotoxicity—casting its shadow upon the neural landscape. In this complex milieu, a subset of PD patients bears witness to a curious phenomenon: a decline in platelet glutamate uptake, a phenomenon that harmonizes with the severity of the disease's impact [17]. Therefore, to investigate the mechanism underlying glutamatergic synapse dysfunction induced by striatal DA neuronal degeneration, it is necessary to confirm the morphological and positional relationship between astrocytes and glutamatergic synapses and the response of astrocytes to DA neuronal degeneration.

In the present study, we employed immunofluorescence and immunoelectron microscopy (IEM) techniques to investigate the morphological association between glutamatergic synaptic terminals and perisynaptic astrocytes. Our objective was to gain insights into the pathological mechanisms underlying the impaired function of striatal glutamatergic synapses in PD.

2. Materials and methods

2.1. Animals and groups

Our animal experiments followed the imperatives outlined in the National Institutes of Health Guide for the Care and Use of Laboratory Animals. The meticulous orchestration and subsequent endorsement occurred under the Animal Care and Use Committee of Jinan University (ethical permission No.: 20200831-14). In the course of this investigation, sixty adult male Sprague–Dawley (SD) rats bearing a weight ranging between 250 and 300 g assumed pivotal roles. Under a meticulously governed 12-h light/dark cycle, nourishment and hydration stood readily accessible. A symphony of randomness allocated these subjects into four distinct cohorts: the normative control group (n = 15), the sham-operation group (n = 15), the vehicle control group (n = 15), and the 6-hydroxydopamine (6OHDA) group (n = 15). Each contingent gave rise to the tapestry of inquiry: six rats for the intricate dance of immunohistochemistry

and immunofluorescence analyses, three subjects as conduits for the meticulous gaze of immunoelectron microscopy (IEM) detection, and yet another cohort of six offered themselves as instruments in the orchestration of Western blotting experiments.

2.2. Surgical operation

The very fabric of our study is interwoven with the PD rat models, whose genesis and essence have been chronicled in antecedent scholarly narratives [5,7,18,19]. In brief, rats in the 6OHDA group received a unilateral injection of 6OHDA (catalog no. H116; Sigma) into the right median forebrain bundle (MFB). Initiating the orchestrated sequence, rats underwent anesthesia using sodium pentobarbital (50 mg/kg, i.p.), subsequently assuming their positions upon the stage of a Kopf stereotaxic instrument (catalog no. 60191, Stoelting Co.). The canvas of their skulls lay bare, coordinates (ML: −1.9 mm, AP: −3.6 mm, DV: −8.2 mm) guiding the narrative. The pivotal moment arrived—the infusion of 8 μl 6OHDA (2.5 μg/μl, dissolved in a 0.9% saline solution enriched with 0.01% ascorbic acid as an antioxidant) into the MFB, executed with the precision of a 10 μl Hamilton syringe. The vehicle control group received an equivalent dose of 0.9% saline solution combined with 0.01% ascorbic acid infused at the same location. For the sham-operation category, the skull was exposed and perforated, yet no treatment regimen ensued. In contrast, the normal control group traversed an alternative course, untouched by surgical procedures or therapeutic interventions. Amidst the temporal expanse of 2–4 weeks post-6OHDA lesions, the rats encountered subcutaneous rendezvous with apomorphine (APO; catalog no. 2073/50, Tocris), rendered at a precise dose of 0.25 mg/kg. A measure of choreography ensued: the tally of 360° contralateral rotations executed within the span of 30 min was meticulously recorded. A decree emerged, resolute in its stance—only those rats orchestrating a tally surpassing 210 rotations would proceed to assume roles in subsequent chapters of inquiry [18]. Furthermore, an intricate choreography unfolded—a spectacle of immunohistochemical prowess. Slices hailing from both the striatum and substantia nigra pars compacta (SNc) danced upon the stage, each bearing the mark of tyrosine hydroxylase (TH) staining. The selection process was unyielding, with only rat models embodying a greater than 90% diminution in TH neurons within the SNc and an 80% decline in TH fibers across the ipsilateral striatum granting passage to the forthcoming chapters of inquiry [18,20,21]. Every rat, an embodiment of eligibility, embarked on a journey of scrutiny, culminating in their sacrifice precisely 28 days postsurgery, thus setting the stage for ensuing analysis.

2.3. Immunohistochemistry, immunofluorescence and IEM

In the symphony of scientific exploration, rats anesthetized with sodium pentobarbital (50 mg/kg, i.p.) embarked on a voyage. Perfusions emerged as a pivotal act—transcardial affairs of 0.9% saline (400 ml), followed by an encore of 400 ml 4% paraformaldehyde-15% saturated picric acid within 0.1 M phosphate buffer (PB; pH 7.4). In parallel, another act unfolded—rats designated for IEM followed a similar course, yet with the addition of 0.6% glutaraldehyde to the fixative. The climax arrived as brains emerged from their bony encasements, embraced by an immersion in 4% paraformaldehyde-15% saturated picric acid within 0.1 M PB at a temperature of 4 °C. Subsequently, a dance of sectioning ensued, orchestrated by the vibratome (catalog no. VT1200S, Leica), resulting in 50 μm slices. The prologue to immunohistochemistry commenced—sections embarking on a sequence of rituals. A prelude of 1% sodium borohydride in 0.1 M PB became, followed by a crescendo of 0.3% hydrogen peroxide (H2O2) in 0.1 M PB (pH 7.4). A 48-h sojourn among 0.1 M PB, housing 1% bovine serum albumin, awaited. This act unfurled in two variations—one replete with the presence of primary antibodies: guinea pig anti-VGlut1 (1:1000, catalog no. AB5905, Millipore), guinea pig anti-VGlut2 (1:2000, catalog no. AB2251-I, Millipore), and mouse anti-GFAP (1:5000, catalog no. MAB3402, Millipore), while the other stood devoid, existing as the negative control ensemble.

For the participants of immunohistochemistry, the stage expanded—secondary antibodies, artists in their own right, took to the spotlight. Biotinylated goat-*anti*-mouse IgG surfaced at a ratio of 1:200 (catalog no. BA9200, VECTOR labs). An overture of rinses followed, as the ensemble ventured through avidin-biotin solution, a sequence of rinses, and immersion within the realm of 0.05% DAB (catalog no. D5637, Sigma) residing within 0.1 M PB. To this mixture, a touch of H_2O_2 was introduced, yielding a final concentration of 0.01%. This journey culminated in a trinity of rinses within 0.1 M PB, setting the stage for the participants designated for the light microscope (LM). This cohort graced gelatin-coated slides, offering themselves to a sequence of stages: air drying, alcohol embrace, xylene caress, and the ultimate shroud of neutral balsam.

The narrative of immunofluorescence, distinct yet intertwined, featured its own chorus. Secondary antibodies, Alexa Fluor 594 and Alexa Fluor 488, lent their luminescent hues to the tale. The visual journey was framed, as sections found their home upon gelatin-coated slides, covered in the embrace of Fluoro-Gel with TES buffer (catalog no. 17985-30, Electron microscopy sciences). Here, fluorescence imagery took center stage, unveiled through the gaze of a laser scanning confocal microscope (LSCM, catalog no. Eclipse Ni-E, Nikon). The essence of double-labeling immunofluorescence was captured within Z-stack digital images, ushering forth the artistry of three-dimensional (3D) reconstruction and measurements through Imaris software (Bitplane, Oxford Instruments Company).

As the narrative shifted toward DAB manifestation, the path diverged into the realm of electron microscopy (EM). Sections found themselves immersed in 0.1 M sodium cacodylate buffer, a precursor to a 1-h rendezvous with 2% osmium tetroxide (OsO4; catalog no. 18456, PELCO) and the same buffer. The sequence progressed, a dance with graded ethyl alcohols, a passage through 1% uranyl acetate within 100% alcohol, culminating in their embrace by EPON 812 resin (catalog no. 18010, PELCO). Ultrathin sections emerged through the agency of an ultramicrotome (catalog no. EM UC6, Leica), and their destiny became mesh grids. Stains of 0.4% lead citrate and 4.0% uranyl acetate swept over these sections, unveiled through the lens of a transmission electron microscope (TEM; catalog no. Tecnai G2 Spirit Twin, FEI company). In this intricate saga, the narrative embraced a multitude of scientific acts, each a brushstroke in the portrait of exploration.

2.4. Western blotting

The Western blotting journey commenced with rats anesthetized by sodium pentobarbital (50 mg/kg, i.p.), leading to decapitation. The striatum was harvested and homogenized, and samples were separated on a 12% SDS–PAGE gel before being transferred onto PVDF membranes (catalog no. IPVH00010, Millipore).

After blocking with 5% nonfat dry milk for 2 h, the membranes were incubated overnight at 4 °C with the following primary antibodies: mouse anti-GFAP (1:5000, catalog no. MAB3402, Millipore), GLAST (1:1000, catalog no. #4166S, CST), GLT1 (1:1000, catalog no. #3838S, CST), GS (1:1000, catalog no. #9832S, CST) and rabbit anti-GAPDH (1:1000, catalog no. mAB5174, CST). Subsequently, horseradish peroxidase (HRP)-conjugated goat anti-mouse IgG (1:200, catalog no. 62–6540, Millipore) was added to the membrane for a 2-h room temperature interaction.

The culmination was achieved through chemiluminescent HRP substrate (catalog no. WBKLs0500, Millipore), which illuminated

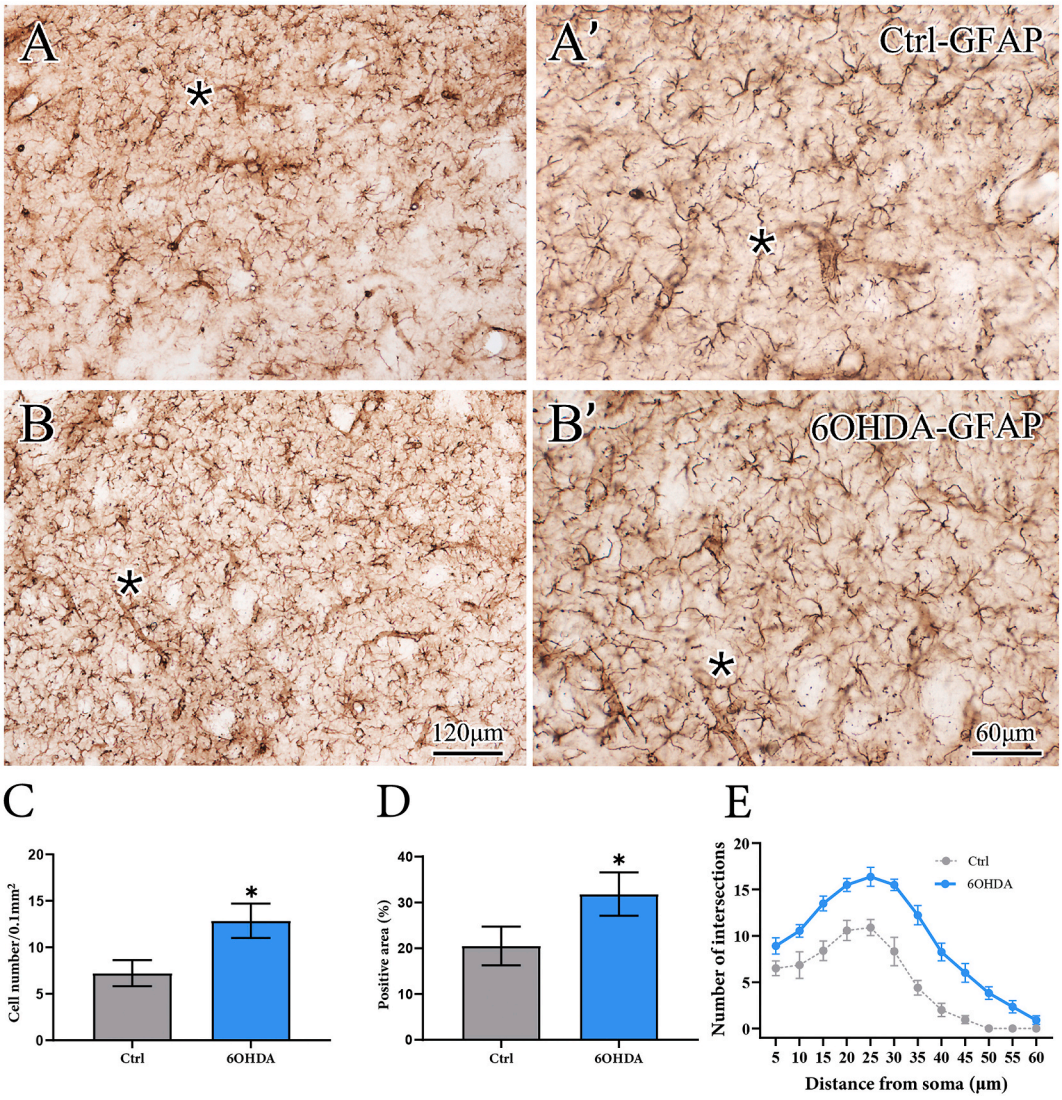

Fig. 1. Morphological changes in striatal astrocytes after DA neuronal degeneration. The morphological attributes exhibited by astrocytes within the control group (depicted in images A and A′) and the 6OHDA group (depicted in images B and B′) are visually represented. Images A′ and B′ are higher magnifications of A and B, and the positions of asterisks (*) in images A and B represent the same positions of asterisks (*) in A′ and B′, respectively. Both image A and image B were captured at identical magnifications, with the scale bar equivalent to 120 μm. Similarly, image a' and image B′ maintain uniform magnification, accompanied by a scale bar denoting 60 μm. To discern disparities between two groups, a student's test (T test) was employed. Image C, the density of astrocytes within the striatal domain exhibited a notable surge subsequent to DA depletion, contrasting the control group. Image D, a conspicuous elevation in the area percentage of GFAP + structures within the 6OHDA group is apparent when juxtaposed with the control cohort. Image E is a Sholl analysis using a two-way analysis of variance (ANOVA). The asterisk (*) emphasizes statistical significance (*$P < 0.05$) between the control and 6OHDA groups.

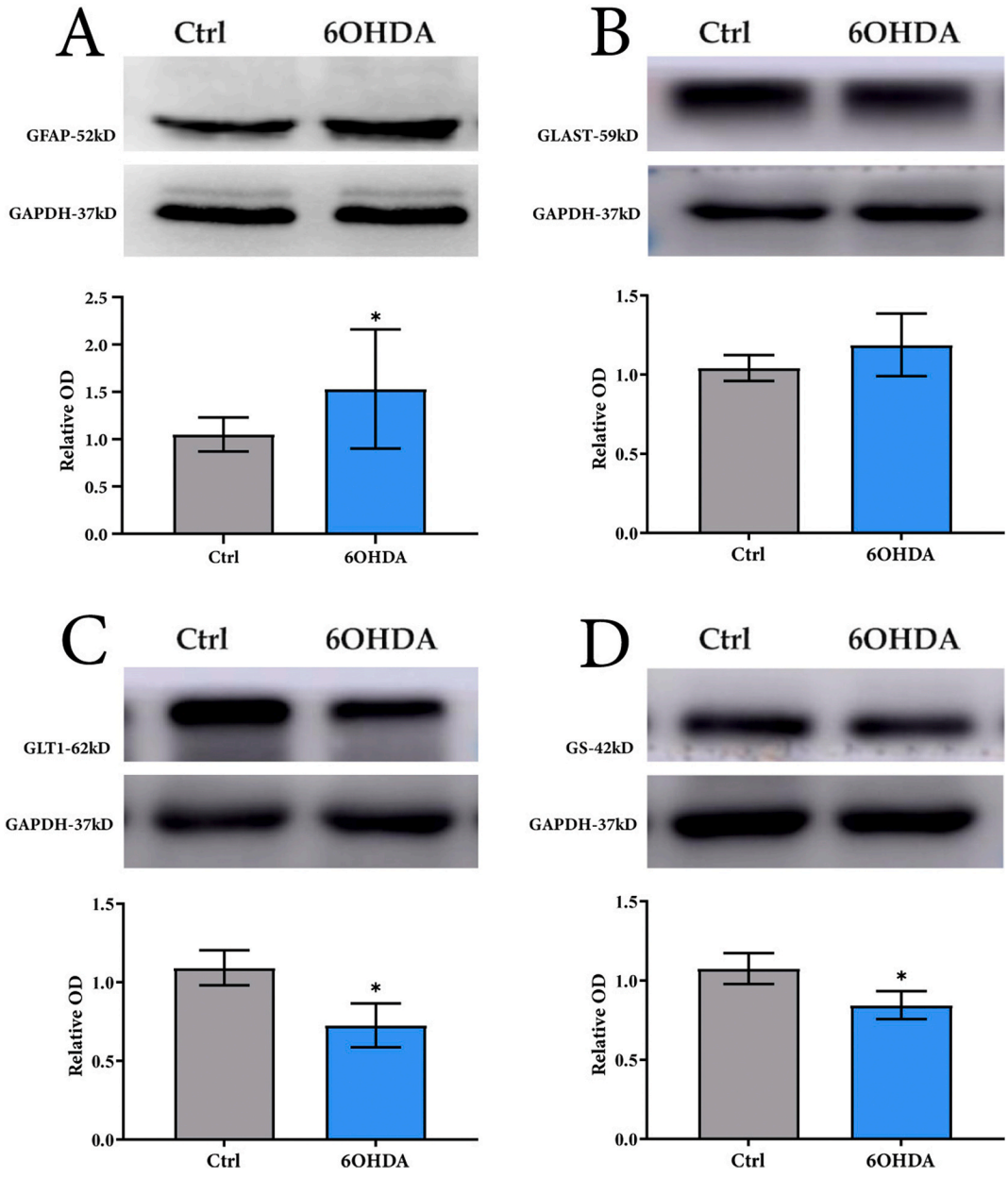

Fig. 2. Western Blotting for GFAP, GLAST, GLT1, GS expressed in astrocytes. Image A (For original uncropped images, see Appendix. Fig. 2A-GFAP and Fig. 2A-GAPDH in the supplementary materials.), western blotting reveals the distinct GFAP protein bands (52KD) across both the control and 6OHDA groups, and we also chart the semi-quantitative outcomes delineating the protein expression levels of GFAP in the two groups using T test. In image B (For original uncropped images, see Appendix. Fig. 2B-GLAST and Fig. 2B-GAPDH in the supplementary materials.), western blotting shows the distinct GLAST protein bands (59KD) across both the control and 6OHDA groups, and we also chart the semi-quantitative outcomes delineating the protein expression levels of GLAST in the two groups using T test. As for image C (For original uncropped images, see Appendix. Fig. 2C-GLT1 and Fig. 2C-GAPDH in the supplementary materials.), western blotting demonstrates the distinct GLT1 protein bands (62KD) across both the control and 6OHDA groups, and we also chart the semi-quantitative outcomes delineating the protein expression levels of GLT1 in the two groups using T test. Finally, in image D (For original uncropped images, see Appendix. Fig. 2D-GS and Fig. 2D-GAPDH in the supplementary materials.), western blotting reveals the distinct GS protein bands (42KD) across both the control and 6OHDA groups, and we also chart the semi-quantitative outcomes delineating the protein expression levels of GS in the two groups using T test, explicitly demonstrating the heightened expression in the 6OHDA group consequent to DA depletion in contrast to the control group. The asterisk (*) emphasizes statistical significance (*$P < 0.05$) between the control and 6OHDA groups.

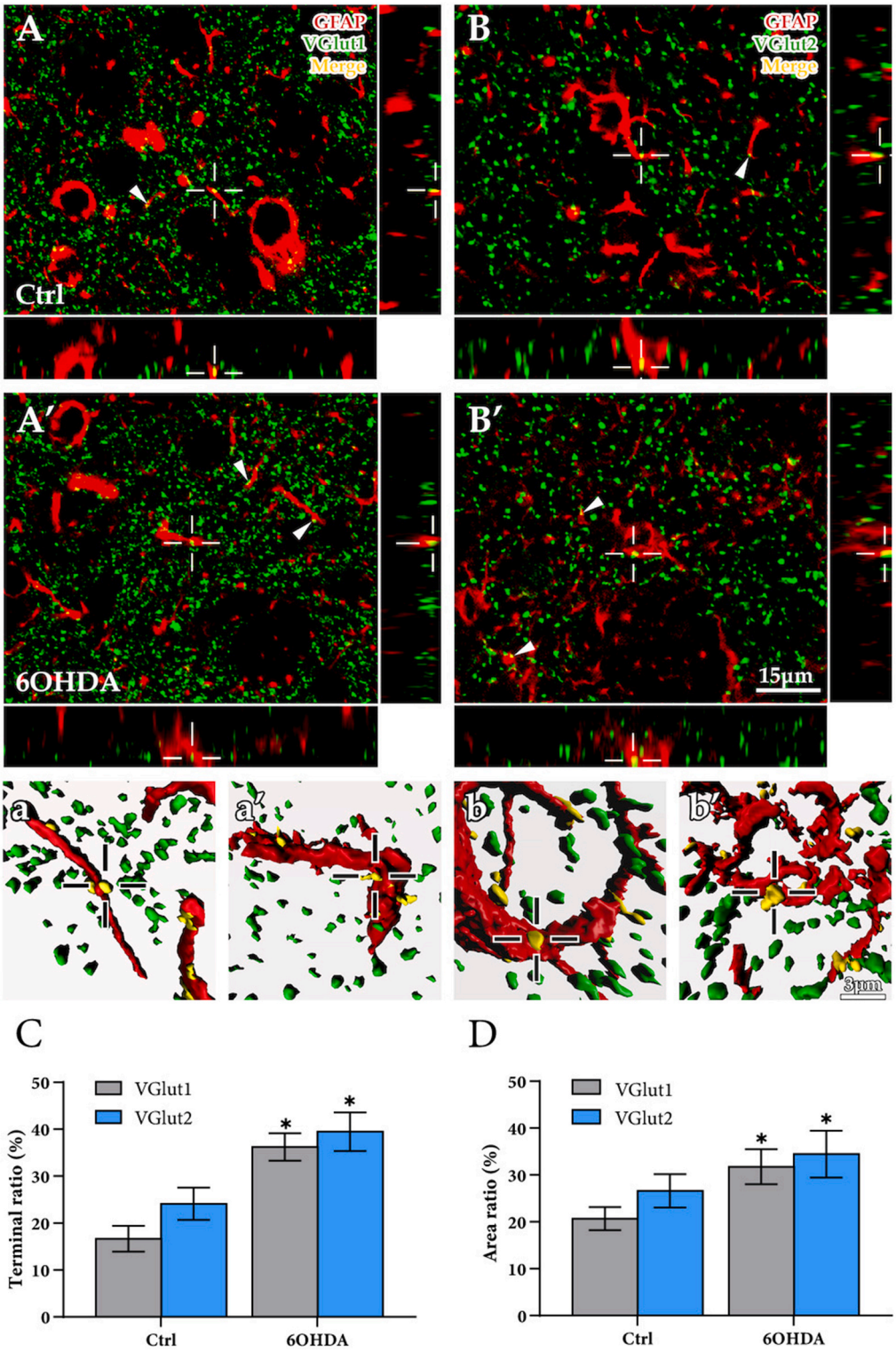

Fig. 3. Double labeling immunofluorescence for astrocytes and VGlut + terminals. Astrocytes (red) and VGlut1+ (green, images A, A′, a, a') or VGlut2+ (green, images B, B′, b, b') formed close appositions (yellow). The white triangle (△) represents VGluts + terminals that are wrapped by astrocytes. The hollow cross symbol (┼) indicates the relationship between the VGluts + terminals and astrocytes in the X, Y, and Z axes. Images a, a', b, b' indicate the 3D reconstruction of terminals and astrocytes, hollow cross (┼) in images a, a', b, b' corresponding to hollow cross (┼) in A, A′, B, B'. Notably, images A, A′, B, and B′ remain consistent in magnification, and their equivalence is underscored by the scale bar set at 15 μm. Similarly, images a, a', b, and b' adhere to an unswerving magnification, accompanied by a scale bar that mirrors a length of 3 μm. Using a two-way

analysis of variance (ANOVA), image C shows the proportion of glutamatergic terminals wrapped by GFAP + astrocytes, and image D indicates the area percentage of VGlut1+ glutamatergic terminals wrapped by GFAP + astrocytes. *P < 0.05, comparison between control group and 6OHDA group. (For interpretation of the references to colour in this figure legend, the reader is referred to the Web version of this article.)

immunoreactive bands, marking the conclusion of the endeavor to discern molecular expression.

2.5. Data collection and statistical analysis

Following the cartography of Paxinos and Watson's revered atlas [22], we embarked on an odyssey through the interaural plane (from 10.70 mm to 8.74 mm). The spotlight fell on the dorsolateral striatal realm, intricately interwoven with the choreography of Parkinson's motor manifestations [23,24]. Across every tier of the striatal hierarchy, contiguous sections bore witness to the vibrant imprint of immunolabeling. VGlut1, VGlut2, and GFAP, like cosmic constellations, adorned the striatal expanse in symphonic harmony. Guided by a veil of blindness, investigators unraveled the tapestry of variances among experimental cohorts.

The orchestration of terminal density quantification ensued, following well-trodden pathways of prior methodologies [7,19,25–27]. Concisely, GFAP + astrocyte density was quantified in five randomly chosen 200 μm-sided squares. IEM data analysis involved random fields in digital EM images. EM analysis was confined to ultrathin sections from the block's upper layers for optimal antibody penetration. VGlut1+ and VGlut2+ terminals were identified through immunoreactivity and vesicle-packed profiles. Detectable spines exhibited diminutive dimensions, linkage to dendrites, prominent postsynaptic density (PSD), or the existence of the spine apparatus. Dendrites were distinguishable due to their size, elongated/oval contour, and structural elements encompassing microtubules and mitochondria. Detailed counting methodologies were established in earlier publications [28–30].

Employing SPSS 20.0 software, the statistical analyses took shape. Experimental data are presented as the mean ± standard deviation (SD). To discern disparities between two groups, a two-way analysis of variance (ANOVA) and Student's T tests were employed accordingly. Throughout these deliberations, a significance level of $P < 0.05$ was the compass guiding the determination of statistical significance.

3. Results

The examination of our experimental data underscored the absence of distinctions among the normal control group, sham-operation group, and vehicle control group (data not displayed). In the interest of sharpening the report's clarity and brevity, the text exclusively showcases data from the vehicle control group and the 6OHDA group, unless expressly indicated otherwise.

3.1. Morphological changes in striatal astrocytes after DA neuronal degeneration

GFAP is a specific marker of astrocytes. Within the scope of this investigation, immunohistochemical analysis unveiled the intricate profiles of GFAP + astrocytes, distinct from neurons in their branching projections, while permeating the striatum with uniformity. In the control group, striatal astrocytes featured diminutive somata accompanied by elongated projections (shown in Fig. 1A, A'). After DA neuronal degeneration, the striatal astrocytes became reactive astrocytes and showed obvious proliferation: the cell body was enlarged, the projections became longer and increasingly thicker, and the number of GFAP + fibers was increased (shown in Fig. 1B, B′). The findings revealed a noteworthy surge in the density of GFAP + cells within the 6OHDA group (12.85 ± 1.85) when juxtaposed with the control group (7.22 ± 1.40, $P < 0.05$, as presented in Fig. 1C). Moreover, the area percentage occupied by GFAP + structures in the 6OHDA group (31.83 ± 4.75%) exhibited a marked elevation in contrast to the control group (20.50 ± 4.23%, $P < 0.05$, as demonstrated in Fig. 1D). Then, we conducted a Sholl analysis using a two-way analysis of variance (ANOVA), which reveals DA neuronal degeneration caused a significant upregulation in the number of astrocyte processes (shown in Fig. 1E)

Aligned with the observed morphological changes, Western blotting analysis revealed an escalated GFAP expression level within the 6OHDA group (1.53 ± 0.63), surpassing that of the control group (1.05 ± 0.18, as displayed in Fig. 2A). This disparity reached statistical significance ($P < 0.05$, as depicted in Fig. 2A). The expression level of GLAST within the 6OHDA Group (1.19 ± 0.19), however, it isn't much higher than the control group (1.04 ± 0.08, $P > 0.05$, as displayed in Fig. 2B). Our research has also found that the expression level of GLT1 in 6OHDA group (0.72 ± 0.13) significantly dropped when compared to the control group (1.09 ± 0.11), which has reached statistical significance ($P < 0.05$, as depicted in Fig. 2C). Similarly, the expression level of GS in 6OHDA group (0.48 ± 0.09) also decreased compared with the control group (1.05 ± 0.09, $P < 0.05$, as depicted in Fig. 2D).

3.2. Effects of DA neuronal degeneration on the morphological relationship between glial cells and glutamatergic synapses

Recent investigations have substantiated the specificity of VGlut1 and VGlut2 antibodies for the distinct immunolabeling of corticostriatal and thalamostriatal terminals, respectively [7,31,32]. According to our previously published studies, DA neuronal degeneration in the striatum significantly upregulated the expression level of VGlut1 in comparison to the control group. And the expression level of VGlut2 protein was also higher in the 6OHDA group than in the control group [6]. Here, fluorescence double-labeled images in the present study showed that a large number of VGluts + axonal terminals were adjacent to GFAP + astrocytes (shown in Fig. 3. A, A′, B, B′). In the control group, 16.66 ± 2.77% of VGlut1+ axonal terminals were adjacent to GFAP + astrocytes (shown in Fig. 3. A, a), and 24.12 ± 3.43% of VGlut2+ axonal terminals were adjacent to GFAP + astrocytes (shown in

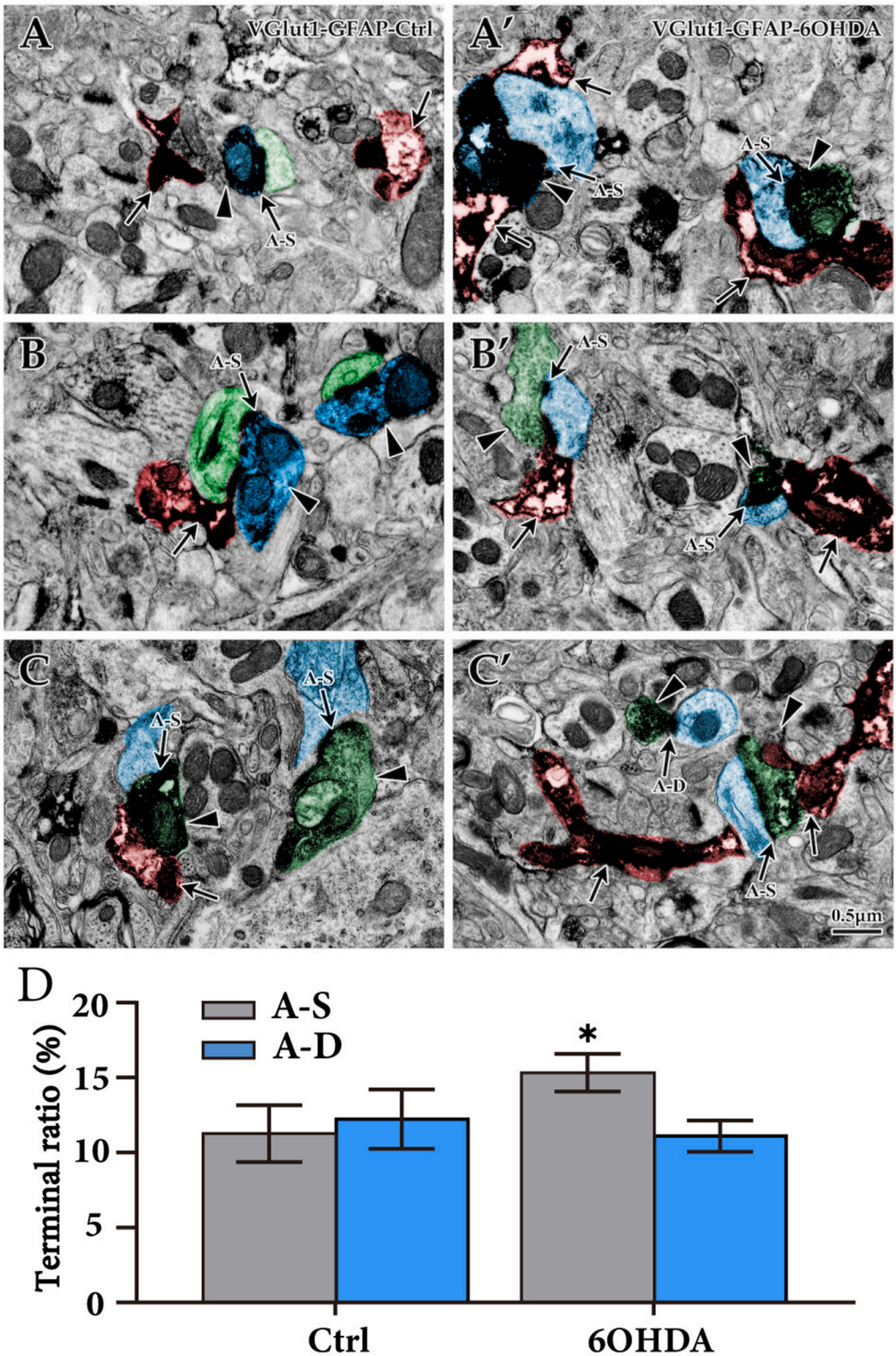

Fig. 4. IEM exploration for morphological changes of perisynaptic astrocytes of VGlut1+ terminals. Depicting the juxtaposition of GFAP + astrocytes and VGlut1+ terminals within the striatal confines, the images are emblematic of the control group (captured in images A, B, C) and the 6OHDA group (mirrored in images A′, B′, C′) as discerned through the technique of dual-labeled immunoelectron microscopy (IEM). The black triangle (▲) represents VGlut1+ terminals, the black arrow (→) represents GFAP + astrocytes, the black arrow with A-S (A-S→) indicates axospinous synapses, and the black arrow with A-D (A-D→) indicates axodendritic synapses. The area marked green is the presynaptic terminals; the area

marked blue is the postsynaptic spine or dendrite; the area marked red is the astrocytes. Uniform in their dimensions and visual scale, each of the images bears an identical magnification factor, accompanied by a scale bar measure of 0.5 μm. To discern disparities between two groups, a two-way analysis of variance (ANOVA) was employed. Throughout these deliberations, a significance level of $P < 0.05$ was the compass guiding the determination of statistical significance. Image D unfurls the panorama of VGlut1+ axo-spinous and axo-dendritic synapses elegantly enshrouded by the embrace of GFAP + astrocytic domains. A–S: axon-spinous synapse; A-D axo-dendritic synapse. *$P < 0.05$, comparison between the control group and the 6OHDA group. (For interpretation of the references to colour in this figure legend, the reader is referred to the Web version of this article.)

Fig. 3. B, b). After 6OHDA treatment, the proportion of glutamatergic terminals wrapped by GFAP + astrocytes were significantly increased (VGlut1: 36.23 ± 2.93%, $P < 0.05$, Fig. 3A', a, 3C; VGlut2: 39.48 ± 4.12%, $P < 0.05$, shown in Fig. 3B', b, 3D).

3D reconstruction of astrocytes and glutamatergic terminals indicated that glutamatergic terminals were wrapped by astrocyte projections to varying degrees. The area percentage of VGlut1+ glutamatergic terminals wrapped by GFAP + astrocytes was higher after 6OHDA treatment (31.75 ± 3.75%, shown in Fig. 3a') than in the control group (20.67 ± 2.46%, $P < 0.05$, shown in Fig. 3a and D). In addition, DA neuronal degeneration induced GFAP + astrocytes to wrap a greater area of VGlut2+ terminals in the 6OHDA group (34.48 ± 5.00%, shown in Fig. 3b') than in the control group (26.63 ± 3.56%, $P < 0.05$, shown in Fig. 3b and D).

To delve into the ultrastructural impact of striatal DA neuronal degeneration on the intricate interplay between VGluts + terminals and astrocytes, we employed a rigorous approach—VGluts and GFAP double-labeled IEM. This method stands as a pivotal tool for verifying the nuanced changes in morphological configurations and spatial associations within the neural landscape. The results revealed that most astrocytes surrounded the synapses, but GFAP + structures were seen on only one side of most synaptic clefts, suggesting that astrocytes may not tightly wrap the synapse across its entire circumference (shown in Figs. 4 and 5). In the control group, 11.27 ± 1.89% of the VGlut1+ axospinous synaptic space was closely adjacent to GFAP + astrocytes (shown in Fig. 4A–C). After 6OHDA treatment, the percentage of VGlut1+ axo-spinous synapses wrapped by GFAP + astrocytes significantly increased (15.33 ± 1.25%, $P < 0.05$, shown in Fig. 4A′-C′, 4D). VGlut2+ axospinous synapses encapsulated by GFAP + astrocytes accounted for 11.70 ± 1.17% of the total synapses in the control group (shown in Fig. 5A–C), and DA neuronal degeneration induced astrocytes to wrap relatively more VGlut2+ axo-spinous synapses (15.35 ± 1.73%, $P < 0.05$, shown in Fig. 5A′-C′, 5D). Nevertheless, the proportions of axo-dendritic synapses labeled with VGlut1+ (11.10 ± 1.04, as depicted in Fig. 4A′-C′) and VGlut2+ (13.42 ± 1.51, as depicted in Fig. 5A′-C′) within the striatum, enshrouded by astrocytic embrace, exhibited no discernible departure from those documented in the control group (VGlut1: 12.23 ± 1.98, $P > 0.05$, as depicted in Fig. 4A–C, 4D; VGlut2: 13.70 ± 1.57, $P > 0.05$, as depicted in Fig. 5A–C, 5D).

4. Discussion

4.1. Striatal glutamate synapses wrapped by astrocytes forming "tripartite synapses"

The brain has two main cellular components: neurons and glial cells. Neurons are thought to be the structural basis of higher brain functions. Glial cells, which outnumber neurons, are thought to serve merely as the "glue" that fills the space between neurons. While the role of glial cells in fundamental support and maintenance remains definitive, emerging indications suggest their entanglement in the dynamic modulation of neuronal activity and synaptic neurotransmission [11]. Astrocytes intricately orchestrate the preservation of synaptic function through the strategic deployment of functional proteins that intricately govern and modulate diverse synaptic processes [33]. Given the contemporary revelations, the presynaptic and postsynaptic membranes, in conjunction with their associated astrocytic counterparts, warrant a comprehensive reevaluation as cohesive entities, designated "tripartite synapses" [34].

Tripartite synapses exhibit distinct morphological characteristics across various brain regions and synapse types. In the cerebellar cortex, astrocytes enwrap all synapses, covering approximately 74% of the Purkinje cell synapse area and only 29% of the pyramidal neuron synapse area [35]. In the hippocampus, astrocytes wrap 57% of the synaptic area. Only 1% of hippocampal synapses are entirely covered by astrocytes, but on average, 43% of the synaptic surface is covered. In this study, we found that striatal glutamatergic synapses were also wrapped by GFAP + astrocyte projections. As a result, in the present study, we used GFAP to show astrocytes. However, while GFAP was a crucial component of the cellular cytoskeleton, it may pose challenges in displaying all the processes of astrocytes. Different types of synapses have varying astrocyte-wrapped proportions and covered areas. For perisynaptic structures, the proportion of thalamostriatal glutamatergic synapses wrapped by astrocytes was slightly higher than that of corticostriatal glutamatergic synapses. Striatal astrocytes show no significant selectivity for postsynaptic structures and encapsulate axo-dendritic and axo-spinous synapses in similar proportions. Perisynaptic astrocytes play a vital role in maintaining synaptic function, and differences in their characteristics may contribute to the varying sensitivities of synapses to injury. Differential alterations in astrocytic wrapping for axo-spinous and axo-dendritic synapses can have significant physiological implications, affecting synaptic plasticity, neuronal communication, and the response to disease or injury. These alterations can influence the formation and function of synapses, and can have a significant impact on learning, memory, and the response to neurological diseases [36].

4.2. Striatal DA neuronal degeneration results in morphological and functional changes in perisynaptic astrocytes

The morphological relationship between astrocytes and synapses also changes with the microenvironment. The pivotal neuropathological hallmark of PD lies in the degeneration of the nigrostriatal dopaminergic pathway, culminating in the marked reduction of DA levels within the striatal domain [6,37]. The consequence of DA neuronal degeneration manifests as aberrant behaviors

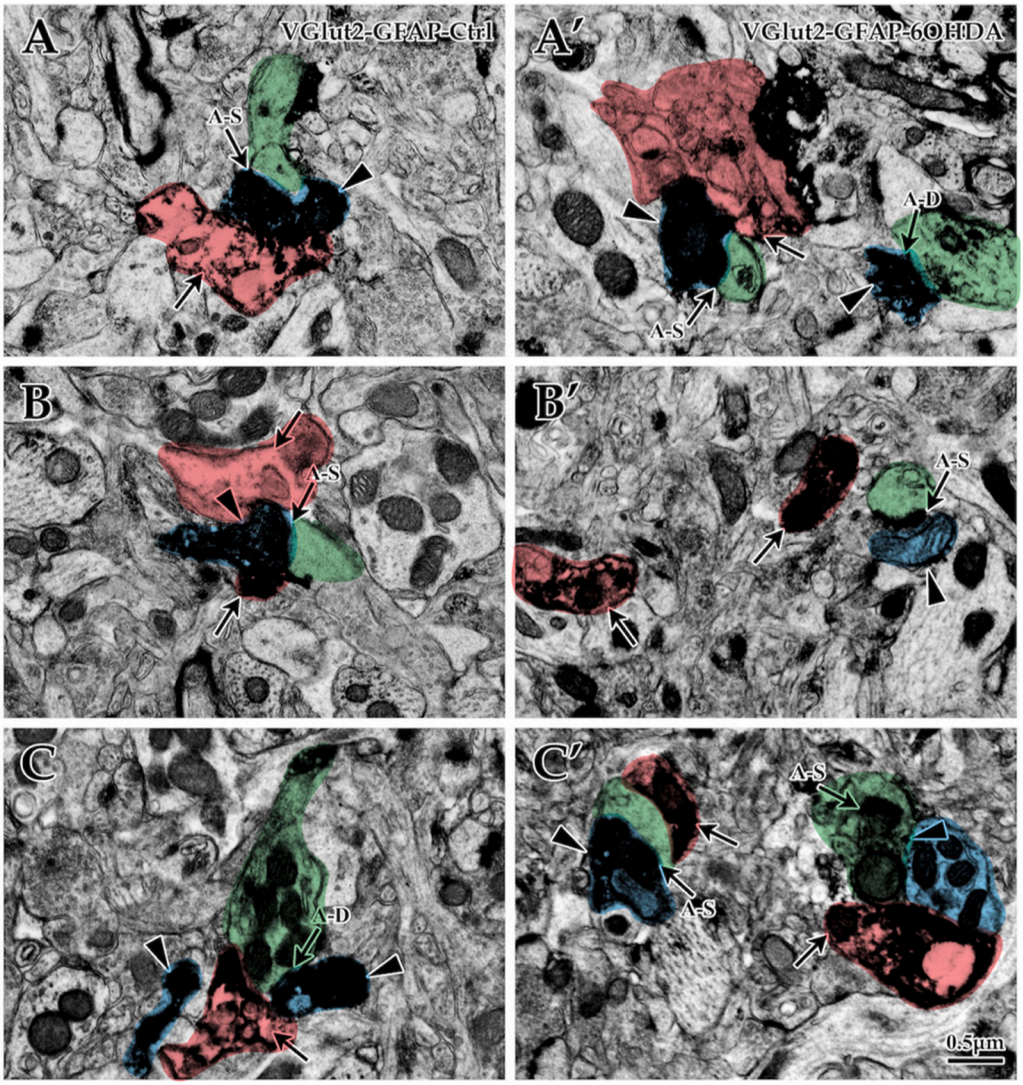

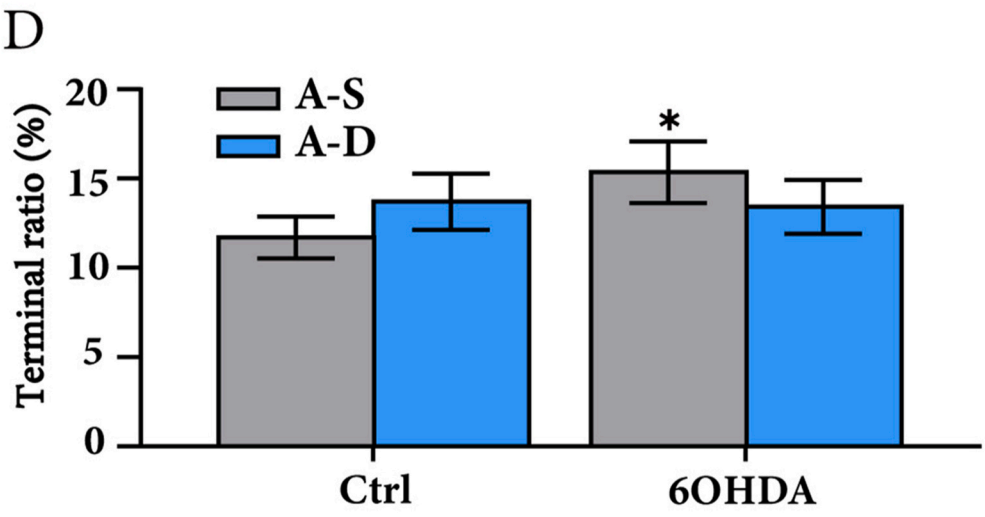

(caption on next page)

Fig. 5. IEM investigation for morphological changes of perisynaptic astrocytes of VGlut2+ terminals. The images vividly portray the intricate juxtaposition of GFAP + astrocytes and VGlut2+ terminals within the striatal domain, as illuminated within the control group (depicted in images A, B, C) and the 6OHDA group (represented by images A′, B′, C′) through the insightful lens of double labeled IEM. The black triangle (▲) represents VGlut1+ terminals, the black arrow (→) represents GFAP + astrocytes, the black arrow with A-S (A-S→) indicates axospinous synapses, and the black arrow with A-D (A-D→) indicates axodendritic synapses. The area marked green is the presynaptic portion; the area marked blue is the postsynaptic version; the area marked red is the astrocytes. Uniform in their dimensions and visual scale, each of the images bears an identical magnification factor, accompanied by a scale bar measure of 0.5 μm. To discern disparities between two groups, a two-way analysis of variance (ANOVA) was employed. Throughout these deliberations, a significance level of $P < 0.05$ was the compass guiding the determination of statistical significance. Image D casts its gaze upon the percentage portrayal of VGlut2+ axo-spinous and axo-dendritic synapses, ensconced within the enigmatic realms of GFAP + astrocytes. A–S: axon-spinous synapse; A-D axo-dendritic synapse. *$P < 0.05$, comparison between the control group and the 6OHDA group. (For interpretation of the references to colour in this figure legend, the reader is referred to the Web version of this article.)

stemming from disrupted striatal function and concurrent apoptotic demise of striatal neurons within PD rat models [18]. Moreover, the presynaptic and postsynaptic structures of tripartite synapses were significantly damaged in PD rat models. Striatal glutamatergic terminals increased in volume and quantity, and the percentage of glutamatergic axo-spinous synapses significantly decreased, but axo-dendritic synapses showed no obvious changes [7]. In addition, postsynaptic components of striatal glutamatergic synapses showed the loss of spines after DA neuronal degeneration [5]. Astrocytes are essential elements of tripartite synapses, and the examination of morphological changes in perisynaptic astrocytes is important for understanding the pathological mechanism involving glutamatergic synapses in the PD striatum. Striatal astrocytes do not thoroughly wrap the synaptic cleft around the entire circumference but cover only part of the synaptic cleft. However, astrocyte protuberances maintain dynamic characteristics, enabling astrocyte morphology to adapt to fluctuations in the microenvironment, including changes in physiological and pathological conditions [9]. This responsivity is attributed to the family of ERM proteins expressed by perisynaptic astrocytes; this family of proteins is also highly expressed in the intestinal epithelium and is generally considered to be the main contributor to microvillus motility [33]. Among individuals afflicted by moderate mesial temporal lobe epilepsy, discernible synaptic expansion becomes apparent, coupled with an augmented frequency of synapses encircled by astrocytes in contrast to those experiencing mild epilepsy. Notably, an affirmative correlation is discerned wherein augmented synaptic volume corresponds to an enlarged region enveloped by astrocytic processes [15]. Consistent with this finding, glutamatergic terminals in the striatum increased after DA neuronal degeneration [7], and the area and proportion wrapped by astrocytes were also increased. Within the perisynaptic milieu, astrocytic entities prominently exhibit the presence of excitatory amino acid transporters (GLAST and GLT1), which are responsible for the immediate sequestration of glutamate residing within the synaptic cleft [11]. This absorption allows astrocytes to deal with excess glutamate in the extracellular space and reduce potential neuronal damage caused by excitotoxicity. Together, GLAST and GLT1 absorb more than 80% of glutamate in synaptic clefts. Our results showed that in rat model of PD, the content and activity of GLT1 were significantly decreased compared with those in normal animals, while the content and activity of GLAST had no significant change. The decreased function of GLT1 may be an important reason for the increase in glutamate concentrations in the extracellular space of the striatum in PD. Overall, the increased glutamate release upon DA neuronal degeneration and the decreased glutamate reabsorption rate caused by decreased astrocyte GLT1 expression may be a significant factor affecting the accumulation of glutamate in the striatum. While the number and area of glutamatergic synapses wrapped by astrocytes increased in PD, these changes were insufficient to restore glutamate to normal levels and prevent neuronal damage. Our research provides novel insights into the role of astrocytes in the pathology of PD. Astrocyte protuberances maintain dynamic characteristics, enabling astrocyte morphology to adapt to fluctuations in the microenvironment. In our study, the upregulation of GLT1 expression in astrocytes under PD conditions facilitates the efficient reuptake of glutamate from the synaptic cleft, acting as a preventive measure against excitotoxic damage. This morphological change in astrocytes affects the reuptake of glutamate, which could potentially contribute to a better understanding of the pathophysiology of PD. Therefore, further reactive astrocytes, or increased GLT1 activity, may be needed to reduce nerve damage induced by excitotoxicity in PD.

In conclusion, astrocytic enwrapping of glutamatergic synapses within the striatum prevails. Under PD conditions, both the structure and functionality of striatal glutamatergic synapses exhibit aberrations, while the spatial interaction between astrocytes and these synapses undergo alteration. In the maintenance of synaptic integrity, astrocytes assert their significance; thus, more studies of the related mechanism is warranted for astrocytic function to be developed as a therapeutic avenue for PD.

Statement of ethics

This study protocol was reviewed and approved by Animal Care and Use Committee of Jinan University, approval number: 20200831-14.

Funding Sources

This work was supported by the National Natural Science Foundation of China (32200832, 82260264), GuangDong Basic and Applied Basic Research Foundation (No. 2020A1515110917), Natural Science Foundation of Guangdong Province (2022A1515012553), Fundamental Research Funds for the Central Universities (No. 11620325), Hunan Provincial Natural Science Foundation of China (2021JJ30561), and Scientific Research Program of Hunan Provincial Education Department (No. 20B469).

Data availability statement

All data generated or analyzed during this study are included in this article, and there's no need to deposit data into a publicly available repository. Further enquiries can be directed to the corresponding author.

CRediT authorship contribution statement

Liping Sun: Writing – original draft, Conceptualization. **Xuefeng Zheng:** Writing – original draft, Investigation, Conceptualization. **Yichen Che:** Writing – review & editing, Investigation. **Ye Zhang:** Visualization, Investigation. **Ziyun Huang:** Data curation. **Linju Jia:** Data curation. **Yaofeng Zhu:** Funding acquisition. **Wanlong Lei:** Resources, Methodology. **Guoqing Guo:** Supervision, Project administration, Methodology. **Chunkui Shao:** Conceptualization, Supervision, Writing – review & editing.

Declaration of competing interest

The authors declare that they have no known competing financial interests or personal relationships that could have appeared to influence the work reported in this paper.

Acknowledgement

All individuals and organizations that had made substantive contributions to this study will be acknowledged in the section Funding Sources.

Appendix A. Supplementary data

Supplementary data to this article can be found online at https://doi.org/10.1016/j.heliyon.2024.e27637.

References

[1] B.R. Bloem, M.S. Okun, C. Klein, Parkinson's disease, Lancet 397 (2021) 2284–2303, https://doi.org/10.1016/S0140-6736(21)00218-X.
[2] Z. Chen, Z.-Y. Zhang, W. Zhang, T. Xie, Y. Li, X.-H. Xu, H. Yao, Direct and indirect pathway neurons in ventrolateral striatum differentially regulate licking movement and nigral responses, Cell Rep. 37 (2021) 109847, https://doi.org/10.1016/j.celrep.2021.109847.
[3] J. Chambon, P. Komal, G.M. Lewitus, G.M. Kemp, S. Valade, H. Adaïdi, N. Al Bistami, D. Stellwagen, Early TNF-dependent regulation of excitatory and inhibitory synapses on striatal direct pathway medium spiny neurons in the YAC128 mouse model of huntington's disease, J. Neurosci. 43 (2023) 672–680, https://doi.org/10.1523/JNEUROSCI.1655-22.2022.
[4] X. Zheng, J. Wu, Y. Zhu, S. Chen, Z. Chen, T. Chen, Z. Huang, J. Wei, Y. Li, W. Lei, A Comparative study for striatal-direct and -indirect pathway neurons to DA depletion-induced lesion in a PD rat model, Neurochem. Int. 118 (2018) 14–22, https://doi.org/10.1016/j.neuint.2018.04.005.
[5] J.D.J. Aceves Buendia, L. Tiroshi, W. Chiu, J.A. Goldberg, Selective remodeling of glutamatergic transmission to striatal cholinergic interneurons after dopamine depletion, Eur. J. Neurosci. 49 (2019) 824–833, https://doi.org/10.1111/ejn.13715.
[6] X. Zheng, Z. Huang, Y. Zhu, B. Liu, Z. Chen, T. Chen, L. Jia, Y. Li, W. Lei, Increase in glutamatergic terminals in the striatum following dopamine depletion in a rat model of Parkinson's disease, Neurochem. Res. 44 (2019) 1079–1089, https://doi.org/10.1007/s11064-019-02739-y.
[7] E. Mercado-Ayón, N. Warren, S. Halawani, L.N. Rodden, L. Ngaba, Y.N. Dong, J.C. Chang, C. Fonck, F. Mavilio, D.R. Lynch, H. Lin, Cerebellar pathology in an inducible mouse model of friedreich ataxia, Front. Neurosci. 16 (2022) 819569, https://doi.org/10.3389/fnins.2022.819569.
[8] C.R. Rose, J.-Y. Chatton, Astrocyte sodium signaling and neuro-metabolic coupling in the brain, Neuroscience 323 (2016) 121–134, https://doi.org/10.1016/j.neuroscience.2015.03.002.
[9] G. Ghézali, G. Dallérac, N. Rouach, Perisynaptic astroglial processes: dynamic processors of neuronal information, Brain Struct. Funct. 221 (2016) 2427–2442, https://doi.org/10.1007/s00429-015-1070-3.
[10] L.P. Diniz, I. Matias, A.P.B. Araujo, M.N. Garcia, F.G.Q. Barros-Aragão, S.V. Alves-Leon, J.M. De Souza, D. Foguel, C.P. Figueiredo, C. Braga, L. Romão, F.C. A. Gomes, α-synuclein oligomers enhance astrocyte-induced synapse formation through TGF-β1 signaling in a Parkinson's disease model, J. Neurochem. 150 (2019) 138–157, https://doi.org/10.1111/jnc.14710.
[11] Y. Wang, A.K.Y. Fu, N.Y. Ip, Instructive roles of astrocytes in hippocampal synaptic plasticity: neuronal activity-dependent regulatory mechanisms, FEBS J. 289 (2022) 2202–2218, https://doi.org/10.1111/febs.15878.
[12] M.A. Petroccione, L.Y. D'Brant, N. Affinnih, P.H. Wehrle, G.C. Todd, S. Zahid, H.E. Chesbro, I.L. Tschang, A. Scimemi, Neuronal glutamate transporters control reciprocal inhibition and gain modulation in D1 medium spiny neurons, Elife 12 (2023) e81830, https://doi.org/10.7554/eLife.81830.
[13] V.A. Selivanov, O.A. Zagubnaya, Y.R. Nartsissov, M. Cascante, Unveiling a key role of oxaloacetate-glutamate interaction in regulation of respiration and ROS generation in nonsynaptic brain mitochondria using a kinetic model, PLoS One 16 (2021) e0255164, https://doi.org/10.1371/journal.pone.0255164.
[14] V.S. Van Laar, N. Roy, A. Liu, S. Rajprohat, B. Arnold, A.A. Dukes, C.D. Holbein, S.B. Berman, Glutamate excitotoxicity in neurons triggers mitochondrial and endoplasmic reticulum accumulation of Parkin, and, in the presence of N-acetyl cysteine, mitophagy, Neurobiol. Dis. 74 (2015) 180–193, https://doi.org/10.1016/j.nbd.2014.11.015.
[15] Y. Jia, S.-J. Mo, Q.-Q. Feng, M.-L. Zhan, L.-S. OuYang, J.-C. Chen, Y.-X. Ma, J.-J. Wu, W.-L. Lei, EPO-dependent activation of PI3K/Akt/FoxO3a signalling mediates neuroprotection in in vitro and in vivo models of Parkinson's disease, J. Mol. Neurosci. 53 (2014) 117–124, https://doi.org/10.1007/s12031-013-0208-0.
[16] Y. Ma, M. Zhan, L. OuYang, Y. Li, S. Chen, J. Wu, J. Chen, C. Luo, W. Lei, The effects of unilateral 6-OHDA lesion in medial forebrain bundle on the motor, cognitive dysfunctions and vulnerability of different striatal interneuron types in rats, Behav. Brain Res. 266 (2014) 37–45, https://doi.org/10.1016/j.bbr.2014.02.039.
[17] F. Hefti, E. Melamed, R.J. Wurtman, Partial lesions of the dopaminergic nigrostriatal system in rat brain: biochemical characterization, Brain Res. 195 (1980) 123–137, https://doi.org/10.1016/0006-8993(80)90871-9.
[18] H. Yuan, S. Sarre, G. Ebinger, Y. Michotte, Histological, behavioural and neurochemical evaluation of medial forebrain bundle and striatal 6-OHDA lesions as rat models of Parkinson's disease, J. Neurosci. Methods 144 (2005) 35–45, https://doi.org/10.1016/j.jneumeth.2004.10.004.

[19] Y.-F. Zhu, W.-P. Wang, X.-F. Zheng, Z. Chen, T. Chen, Z.-Y. Huang, L.-J. Jia, W.-L. Lei, Characteristic response of striatal astrocytes to dopamine depletion, Neural Regen. Res. 15 (2020) 724, https://doi.org/10.4103/1673-5374.266917.
[20] A.C. Kreitzer, Physiology and pharmacology of striatal neurons, Annu. Rev. Neurosci. 32 (2009) 127–147, https://doi.org/10.1146/annurev.neuro.051508.135422.
[21] A.H. Gittis, A.C. Kreitzer, Striatal microcircuitry and movement disorders, Trends Neurosci. 35 (2012) 557–564, https://doi.org/10.1016/j.tins.2012.06.008.
[22] S. Mu, L. OuYang, B. Liu, Y. Zhu, K. Li, M. Zhan, Z. Liu, Y. Jia, W. Lei, Protective effect of melatonin on 3-NP induced striatal interneuron injury in rats, Neurochem. Int. 59 (2011) 224–234, https://doi.org/10.1016/j.neuint.2011.05.009.
[23] S. Mu, E. Lin, B. Liu, Y. Ma, L. OuYang, Y. Li, S. Chen, J. Zhang, W. Lei, Melatonin reduces projection neuronal injury induced by 3-nitropropionic acid in the rat striatum, Neurodegener. Dis. 14 (2014) 139–150, https://doi.org/10.1159/000365891.
[24] Y. Nakano, F. Karube, Y. Hirai, K. Kobayashi, H. Hioki, S. Okamoto, H. Kameda, F. Fujiyama, Parvalbumin-producing striatal interneurons receive excitatory inputs onto proximal dendrites from the motor thalamus in male mice, J. Neurosci. Res. 96 (2018) 1186–1207, https://doi.org/10.1002/jnr.24214.
[25] Y.P. Deng, T. Wong, C. Bricker-Anthony, B. Deng, A. Reiner, Loss of corticostriatal and thalamostriatal synaptic terminals precedes striatal projection neuron pathology in heterozygous Q140 Huntington's disease mice, Neurobiol. Dis. 60 (2013) 89–107, https://doi.org/10.1016/j.nbd.2013.08.009.
[26] W. Lei, Y. Deng, B. Liu, S. Mu, N.M. Guley, T. Wong, A. Reiner, Confocal laser scanning microscopy and ultrastructural study of VGLUT2 thalamic input to striatal projection neurons in rats, J. Comp. Neurol. 521 (2013) 1354–1377, https://doi.org/10.1002/cne.23235.
[27] W. Lei, Y. Jiao, N. Del Mar, A. Reiner, Evidence for differential cortical input to direct pathway versus indirect pathway striatal projection neurons in rats, J. Neurosci. 24 (2004) 8289–8299, https://doi.org/10.1523/JNEUROSCI.1990-04.2004.
[28] A. Kashani, C. Betancur, B. Giros, E. Hirsch, S.E. Mestikawy, Altered expression of vesicular glutamate transporters VGLUT1 and VGLUT2 in Parkinson disease, Neurobiol. Aging 28 (2007) 568–578, https://doi.org/10.1016/j.neurobiolaging.2006.02.010.
[29] X. Zheng, L. Sun, B. Liu, Z. Huang, Y. Zhu, T. Chen, L. Jia, Y. Li, W. Lei, Morphological study of the cortical and thalamic glutamatergic synaptic inputs of striatal parvalbumin interneurons in rats, Neurochem. Res. 46 (2021) 1659–1673, https://doi.org/10.1007/s11064-021-03302-4.
[30] A. Derouiche, E. Anlauf, G. Aumann, B. Mühlstädt, M. Lavialle, Anatomical aspects of glia–synapse interaction: the perisynaptic glial sheath consists of a specialized astrocyte compartment, J. Physiol. Paris 96 (2002) 177–182, https://doi.org/10.1016/S0928-4257(02)00004-9.
[31] A. Araque, V. Parpura, R.P. Sanzgiri, P.G. Haydon, Tripartite synapses: glia, the unacknowledged partner, Trends Neurosci. 22 (1999) 208–215, https://doi.org/10.1016/s0166-2236(98)01349-6.
[32] J. Spacek, Three-dimensional analysis of dendritic spines. III. Glial sheath, Anat. Embryol. 171 (1985) 245–252, https://doi.org/10.1007/BF00341419.
[33] C. Venkateshappa, G. Harish, R.B. Mythri, A. Mahadevan, M.M. Srinivas Bharath, S.K. Shankar, Increased oxidative damage and decreased antioxidant function in aging human substantia nigra compared to striatum: implications for Parkinson's disease, Neurochem. Res. 37 (2012) 358–369, https://doi.org/10.1007/s11064-011-0619-7.
[34] B.G. Garcia, M.D. Neely, A.Y. Deutch, Cortical regulation of striatal medium spiny neuron dendritic remodeling in parkinsonism: modulation of glutamate release reverses dopamine depletion–induced dendritic spine loss, Cerebr. Cortex 20 (2010) 2423–2432, https://doi.org/10.1093/cercor/bhp317.
[35] S. Zaja-Milatovic, D. Milatovic, A.M. Schantz, J. Zhang, K.S. Montine, A. Samii, A.Y. Deutch, T.J. Montine, Dendritic degeneration in neostriatal medium spiny neurons in Parkinson disease, Neurology 64 (2005) 545–547, https://doi.org/10.1212/01.WNL.0000150591.33787.A4.
[36] Y. Danjo, E. Shigetomi, Y.J. Hirayama, K. Kobayashi, T. Ishikawa, Y. Fukazawa, K. Shibata, K. Takanashi, B. Parajuli, Y. Shinozaki, S.K. Kim, J. Nabekura, S. Koizumi, Transient astrocytic mGluR5 expression drives synaptic plasticity and subsequent chronic pain in mice, J. Exp. Med. 219 (2022) e20210989, https://doi.org/10.1084/jem.20210989.
[37] Y. Shen, P. He, Y. Fan, J. Zhang, H. Yan, W. Hu, H. Ohtsu, Z. Chen, Carnosine protects against permanent cerebral ischemia in histidine decarboxylase knockout mice by reducing glutamate excitotoxicity, Free Radic. Biol. Med. 48 (2010) 727–735, https://doi.org/10.1016/j.freeradbiomed.2009.12.021.